

A Series of Cu^I Complexes Containing 1,10-Phenanthroline Derivative Ligands: Synthesis, Characterization, Photophysical, and Oxygen-Sensing Properties

Linfang Shi^[a,b] and Bin Li^{*[a]}

Keywords: Luminescence / Copper / N ligands / Sensors

Five novel copper(I) complexes with the general formula [Cu(dpephos)(NN)]BF₄ {dpephos = bis[2-(diphenylphosphanyl)phenyl] ether, NN = 2-phenyl-1*H*-imidazo[4,5-*f*][1,10]phenanthroline (pip, **1**), 1-ethyl-2-phenyl-1*H*-imidazo[4,5-*f*][1,10]phenanthroline (epip, **2**), 2-(naphthalen-1-yl)-1*H*-imidazo[4,5-*f*][1,10]phenanthroline (nip, **3**), 1-ethyl-2-(naphthalen-1-yl)-1*H*-imidazo[4,5-*f*][1,10]phenanthroline (enip, **4**), 2-(anthracen-9-yl)-1-ethyl-1*H*-imidazo[4,5-*f*][1,10]phenanthroline (aeip, **5**)} were rationally designed and synthesized, and these complexes were characterized by ¹H NMR and IR spectroscopy and elemental analysis. X-ray crystal-structure analysis of **3** and **4** are also presented. Their photophysical properties at room temperature were examined by

using a combination of cyclic voltammetry and electronic absorption spectroscopy. It was found that **1–4** display broad-band emission in the solid state upon excitation at $\lambda = 400$ nm, and the emission maxima are located in the range 530–558 nm; the excited-state lifetimes of these complexes are 8.24, 1.97, 6.99, and 2.43 μ s, respectively. As a result, the emission intensity of complexes **1–4** is sensitive to oxygen concentration, and they display oxygen-sensing properties after they are encapsulated into mesoporous silica MCM-41 or SBA-15.

(© Wiley-VCH Verlag GmbH & Co. KGaA, 69451 Weinheim, Germany, 2009)

Introduction

The photophysics of luminescent copper(I) complexes has been the object of intensive investigation for the past decades. Thanks to the pioneering work, the mechanism of emission and quenching of luminescent copper(I) complexes has been studied systematically.^[1] In comparison to some transition-metal complexes, copper(I)-based ones are less toxic, inexpensive, and less environmentally hazardous. These advantages make their practical application possible. Recently, much effort has been devoted to the exploration of the applications of copper(I) complexes in solar energy conversion, biological probing, and organic light-emitting devices (OLEDs).^[2] Luminescence-based oxygen sensing is another important application for luminescent metal complexes, because the determination of the concentration of oxygen in gaseous and aqueous samples and in biological fluids has great significance. Oxygen is a powerful quencher of the emission intensity and excited-state lifetime of some luminescent complexes. Several metal complexes have been

tested as oxygen-sensing probes and some of them displayed excellent performance.^[3] However, few reports on the application of copper complexes in oxygen sensing have been published so far.^[4]

In order to examine the possibility of practical application of complexes based on this inexpensive metal in oxygen sensing, we synthesized a series of copper(I) complexes abbreviated as [Cu(dpephos)(NN)]BF₄ {dpephos = bis[2-(diphenylphosphanyl)phenyl] ether, NN = 2-phenyl-1*H*-imidazo[4,5-*f*][1,10]phenanthroline (pip, **1**), 1-ethyl-2-phenyl-1*H*-imidazo[4,5-*f*][1,10]phenanthroline (epip, **2**), 2-(naphthalen-1-yl)-1*H*-imidazo[4,5-*f*][1,10]phenanthroline (nip, **3**), 1-ethyl-2-(naphthalen-1-yl)-1*H*-imidazo[4,5-*f*][1,10]phenanthroline (enip, **4**), 2-(anthracen-9-yl)-1-ethyl-1*H*-imidazo[4,5-*f*][1,10]phenanthroline (aeip, **5**)} and studied their photophysical and oxygen-sensing properties. For practical applications in optical oxygen-sensing devices, it is necessary to incorporate the dye molecules into a solid matrix that can act as a medium for supporting the dye molecules and for oxygen transportation from the environment. There are many reports on luminescence-based oxygen sensors utilizing different matrixes,^[3f,5] from which can be concluded that the support does indeed have quite stringent criteria for suitable performance. Additionally, for a suitable matrix, it must lend itself to convenient attachment to the sensor probe. Mesoporous silica particles are able to physically encapsulate and immobilize the probe molecules in the pores; furthermore, the existence of channels in these materials allows the transportation of small molecules including molec-

[a] Key Laboratory of Excited State Processes, Changchun Institute of Optics, Fine Mechanics and Physics, Chinese Academy of Sciences,

Changchun 130033, P. R. China

Fax: +86-431-84627031

E-mail: lib020@yahoo.cn

[b] Graduate School of the Chinese Academy of Sciences, Chinese Academy of Sciences,

Beijing 100039, P. R. China

Supporting information for this article is available on the WWW under <http://www.eurjic.org> or from the author.

ular oxygen into the mesoporous materials. So, the luminescence of probe molecules incorporated into mesoporous silica could be quenched readily by oxygen molecules surrounding it.

In light of the reasons mentioned above, we choose mesoporous silica mobil catalytic material 41(MCM-41) and Santa Barbara amorphous 15 (SBA-15) as matrix, because they possess high surface area and periodic nanoscale pores that will facilitate the adsorption and desorption of oxygen. We have conventionally encapsulated this series of copper(I) complexes into the well-studied mesoporous silica MCM-41 and SBA-15 by a physical incorporation technique and tested their oxygen-sensing properties. The results of the experiments indicate that complexes **1–4** possess oxygen-sensing properties after incorporation into such a matrix.

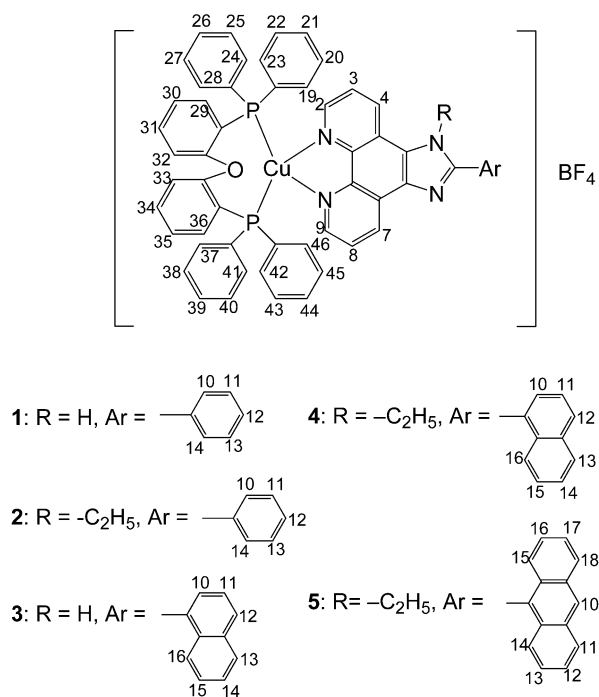
Results and Discussion

Synthesis and Characterization

The NN ligands and the corresponding copper(I) complexes were prepared according to a reported method with some modification.^[6] Both the ligands and the complexes were characterized by ¹H NMR and IR spectroscopy and elemental analysis. The aromatic protons of dpephos in [Cu(dpephos)(NN)]BF₄ appear as complex sets of multiplets (some overlapping) in the region $\delta = 7.324$ to 6.285 ppm. The existence of dpephos can be further confirmed by IR spectroscopy: 1265, 1263, 1263, 1261, 1261 cm⁻¹ for **1–5**, respectively, which should be attributed to the stretching vibration of Ar–O–Ar. The absorption lo-

cated at 1433 ± 3 cm⁻¹ is a characteristic vibration of P–Ar. The presence of aryl groups in the ligands and **1–5** is confirmed by the absorptions at 737–747 and 3053 ± 4 cm⁻¹, which should be attributed to the out-of-plane deformation of C–H and the stretching vibration of =C–H, respectively. The absorption located at 1562 cm⁻¹ in the NN ligands is characteristic of C=C vibrations, and as for complexes **1–5**, this kind of vibration is in the region 1564–1579 cm⁻¹. The IR spectra of the five complexes together with those of the NN ligands also include the characteristic absorption of C=N stretching vibrations located in the region 1595–1627 cm⁻¹. The presence of the [BF₄]⁻ anion was found in the IR spectra with the $\nu(\text{B–F})$ mode at 1074, 1055, 1070, 1058, and 1054 cm⁻¹ for complexes **1–5**, respectively.^[6a] Scheme 1 depicts the molecular structures of this series of complexes.

For further confirmation of the structure of the complexes, single crystals of **3**·6C₂H₅OH and **4**·2C₂H₅OH were selected for X-ray diffraction analysis. The former crystal was measured at 273 K and the latter was measured at



Scheme 1. Molecular structures of **1–5**.

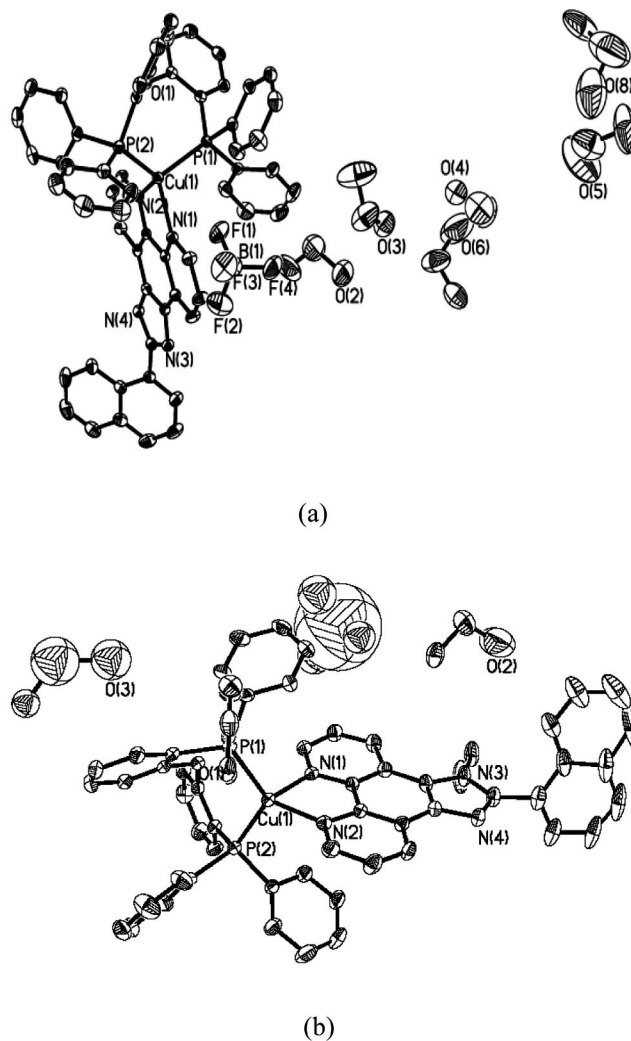


Figure 1. ORTEP drawing of crystals of (a) **3**·6C₂H₅OH and (b) **4**·2C₂H₅OH with displacement ellipsoids at the 30% probability level. Hydrogen atoms are omitted for clarity.

153 K. Being exposed to air at room temperature for 5 h, they lost solvent molecules and the framework of the single crystals was broken down.

Single-crystal X-ray structure determinations of $3 \cdot 6\text{C}_2\text{H}_5\text{OH}$ and $4 \cdot 2\text{C}_2\text{H}_5\text{OH}$ show that the copper(I) ion is in a N2P2 distorted tetrahedral environment in which the dpephos ligand was bound through its pair of P donor atoms and the phenanthroline derivative through two dimine N atoms. Crystal data and refinement details for $3 \cdot 6\text{C}_2\text{H}_5\text{OH}$ and $4 \cdot 2\text{C}_2\text{H}_5\text{OH}$ are presented in Table S1 (Supporting Information). The ORTEP representations of these structures are shown in Figure 1, whereas selected bond lengths and bond angles are given in Table 1. It is clearly seen from the data summarized in Table 1 that the Cu–N bond lengths are almost identical in the two complexes, as are those of Cu–P. The Cu–N and Cu–P distances are within the normal range.^[1e,1f,6a] The distortion presumably arises from the restricted bite angle of the NN ligand N(1)–Cu(1)–N(2) 80.84(11)° for $3 \cdot 6\text{C}_2\text{H}_5\text{OH}$ and 80.48(18)° for $4 \cdot 2\text{C}_2\text{H}_5\text{OH}$, whereas the corresponding diphosphane bite angle P(1)–Cu(1)–P(2) is 113.67(4)° for $3 \cdot 6\text{C}_2\text{H}_5\text{OH}$ and 118.05(6)° for $4 \cdot 2\text{C}_2\text{H}_5\text{OH}$. The dihedral angle between the Cu–N(1)–N(2) and Cu–P(1)–P(2) planes is 87.28° for $3 \cdot 6\text{C}_2\text{H}_5\text{OH}$ and 89.62° for $4 \cdot 2\text{C}_2\text{H}_5\text{OH}$, which indicates that the two planes are almost perpendicular.

Table 1. Selected bond lengths [Å] and angles [°] for complexes $3 \cdot 6\text{C}_2\text{H}_5\text{OH}$ and $4 \cdot 2\text{C}_2\text{H}_5\text{OH}$.^[a]

$3 \cdot 6\text{C}_2\text{H}_5\text{OH}$		$4 \cdot 2\text{C}_2\text{H}_5\text{OH}$	
Cu(1)–N(1)	2.058(3)	Cu(1)–N(1)	2.074(4)
Cu(1)–N(2)	2.070(3)	Cu(1)–N(2)	2.036(5)
Cu(1)–P(1)	2.2697(10)	Cu(1)–P(1)	2.2259(16)
Cu(1)–P(2)	2.2273(10)	Cu(1)–P(2)	2.2539(17)
N(1)–Cu(1)–N(2)	80.84(11)	N(1)–Cu(1)–N(2)	80.48(18)
N(1)–Cu(1)–P(1)	124.87(9)	N(2)–Cu(1)–P(1)	122.57(15)
N(2)–Cu(1)–P(1)	116.11(8)	N(1)–Cu(1)–P(1)	109.14(13)
N(1)–Cu(1)–P(2)	108.14(8)	N(2)–Cu(1)–P(2)	113.11(14)
N(2)–Cu(1)–P(2)	108.39(8)	N(1)–Cu(1)–P(2)	104.45(14)
P(2)–Cu(1)–P(1)	113.67(4)	P(1)–Cu(1)–P(2)	118.05(6)

[a] Numbers in parentheses are estimated standard deviations in the least significant digits.

Thermal Stability

Thermogravimetric analysis (TGA) was performed on the powder samples of **1–5** under a nitrogen atmosphere to investigate their stable characteristics, and the TGA traces of the five complexes are presented in Figure 2. Complex **1** began to lose weight when it was heated to 222 °C, which should be attributed to the loss of the diphenyl ether moiety of dpephos. The thermal characteristics of **2** are similar to those of **1**: it began to decompose gradually at 231 °C and totally lost the diphenyl ether group at 391 °C. Complex **3** began to decompose at ca. 260 °C, and when it was heated to 410 °C, diphenyl ether and the other four phenyl groups of the dpephos ligand were completely lost. As can be seen from their TGA traces, the thermal stability of **4** and **5** is better than that of **1**, **2**, and **3**. The initial temperature of

weight lost for **4** and **5** is ca. 312 and ca. 249 °C, respectively, and the temperatures of complete loss of the diphenyl ether and other phenyl groups of dpephos for **4** and **5** are ca. 413 and ca. 412 °C, respectively. At temperature higher than 500 °C, all five compounds began to dramatically dissociate. When the temperature reached ca. 600 °C, the compounds totally decomposed and only CuBF_4 remained.

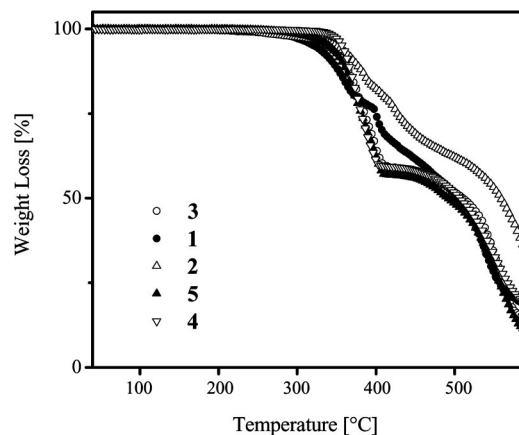


Figure 2. TGA curves of **1–5**.

Photophysical Properties

As shown in Figure S1 (Supporting Information), the absorption spectra of **1–5** recorded in CH_2Cl_2 exhibit intense π – π^* ligand-centered bands in the region 220–350 nm and weak and broad metal-to-ligand charge-transfer (MLCT) bands with an onset at 450, 470, 460, 460, and 490 nm for **1–5**, respectively. The absorption maxima in the visible region for **1–4** are 413, 407, 408, and 407 nm, respectively, whereas complex **5** exhibits no absorption maximum in this region. Their molar absorption coefficients are compiled in Table 2.

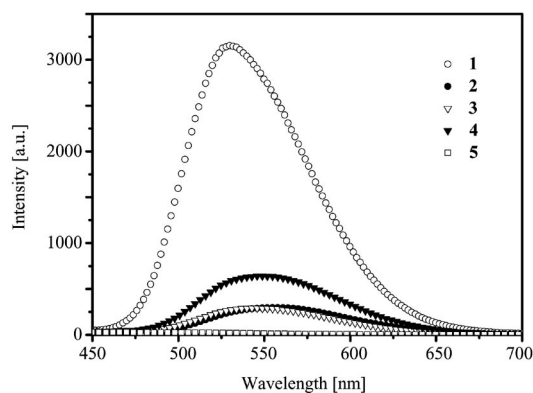
In air-equilibrated CH_2Cl_2 solutions, all five complexes exhibit no luminescence, which is similar to that of $[\text{Cu}(\text{dpephos})(1,10\text{-phenanthroline})]\text{BF}_4$.^[6a] In the solid state, **1–4** exhibit luminescence from the MLCT excited states. For comparison purposes, the emission spectra of the five complexes in the solid state at room temperature are presented in Figure 3 and the solid-state photoluminescence quantum yield of **1–4** are compiled in Table 2. Upon excitation at $\lambda = 400$ nm, powders of **1–4** show broad band emission at $\lambda_{\text{max}} = 530, 558, 543,$ and 548 nm, respectively, whereas the emission intensity is strikingly different: $1 \gg 4 > 3 \approx 2$. The emission of **5** is extremely weak relative to that of **1–4**. As a result, we have not obtained its solid-state photoluminescence lifetime decay and quantum yield data. As shown in Figure S2 (Supporting Information), the photoluminescence spectra of **1–4** are composed of two exponential decays, and the values are in the order of microseconds. The average excited-state lifetimes (τ) of **1–4** are presented in Table 2.

Because all of the emission spectra are recorded under the same conditions, the differences in the emission spectra

Table 2. Photophysical characteristics of **1–5**.

Complex	$\lambda_{\text{max,abs}}$ [nm] ^[a]	[L mol ⁻¹ cm ⁻¹]	$\lambda_{\text{max,em}}$ [nm] ^[b]	Φ ^[c]	τ [μ s] ^[d]
1	226	81100	530	0.14	8.24
	281	88520			
	413	8450			
2	226	147820	558	0.02	1.97
	270	156110			
	407	15020			
3	227	103780	543	0.02	6.99
	262	65910			
	295	58100			
4	226	135740	548	0.04	2.43
	259	82010			
	288	63820			
5 ^[e]	407	7180			
	227	71590			
	256	194540			
	286	35050			
	350	11280			
	368	14760			
	389	14880			

[a] Measured from dichloromethane with the concentration of 1×10^{-5} mol L⁻¹. [b] Solid-state emission maxima of the complexes. [c] The photoluminescence quantum yield calculated according to a literature method.^[10] [d] Solid-state excited-state lifetime measured on powder samples of **1–4**. [e] No absorption peak in the visible region was observed. As a result of its extremely weak emission, photoluminescence lifetime decay and quantum yield data have not been obtained.

Figure 3. Emission spectra of **1–5** in the solid state at room temperature upon excitation at $\lambda = 400$ nm.

should be attributed to their molecular structure. The five complexes contain an identical phosphane ligand (i.e., dpephos), and only the structures of the NN ligands are different. As presented in Scheme 1, the molecular back-

bone of pip mainly consists of an imidazo ring, a phenyl ring, and a phenanthroline ring. As for nip, enip, and aeip, the substitution group at the 2-position of the imidazo ring is naphthyl and anthryl, respectively. The imidazo[4,5-*f*]-[1,10] phenanthroline moiety of the pip molecule is coplanar with the phenyl ring, and as for epip, this moiety is not coplanar with the phenyl ring as a result of the grating of the ethyl group to the nitrogen atom on the imidazo ring,^[7] thus, the pip molecule is more flattened than epip. A flattening of the ligand will lead to extended intraligand electron delocalization and minimized excited-state distortion of the corresponding complex.^[8] This is not only the reason why **1** exhibits higher emission intensity and energy than **2** does, but also the cause for its exhibiting the strongest emission and highest emission energy among the five complexes. The imidazo[4,5-*f*]-1,10-phenanthroline moiety is not coplanar with the naphthyl and anthryl ring in nip, enip, or aeip. The dihedral angles between the imidazo ring and the aryl group is 40.4, 76.36, and 83.63° for nip, enip, and aeip, respectively. In particular, the two planes are almost perpendicular in aeip, which results in the worst coplanarity of the NN ligand, and thus, the weakest emission of **5** among the series of complexes is not a surprise. As for the difference in emission intensity between **3** and **4** (i.e., **4** > **3**), it should be the effect of the ethyl substituent in enip that can presumably decrease the energy loss coming from N–H vibration.^[9]

Cyclic Voltammetry

Cyclic voltammograms of complexes **1**, **2**, **4**, and **5** exhibit irreversible metal-centered oxidation and ligand-based reduction behavior in CH₃CN solution, which are in consistent with phenanthroline-based Cu^I diimine complexes reported in the literature.^[11,12] The reduction process of **3** appears reversible, whereas the oxidation process is irreversible. Their onset oxidation and reduction potential vs. SCE are summarized in Table 3.

The energy levels of the highest-occupied molecular orbital (HOMO) and the lowest-unoccupied molecular orbital (LUMO) are calculated from the onset oxidation [$E_{\text{onset(Ox)}}$] and reduction [$E_{\text{onset(Red)}}$] potentials with the formula $E_{\text{HOMO}} = -4.74 - E_{\text{onset(Ox)}}$ (–4.74 V for SCE with respect to the zero vacuum level) and $E_{\text{LUMO}} = -4.74 - E_{\text{onset(Red)}}$.^[12] The data of E_{HOMO} , E_{LUMO} , and gaps between the LUMO and HOMO energy levels are presented in Table 3. These values are in good agreement with those obtained from UV/Vis spectroscopy.

Table 3. Electrochemical data for **1–5**.

	$V_{1/2}$ [V]	$E_{\text{onset(Ox)}}$ [V]	$E_{1/2}$ [V]	$E_{\text{onset(Red)}}$ [V]	E_{HOMO} [eV]	E_{LUMO} [eV]	E_{get} [eV] ^[a]	E_{gpt} [eV] ^[b]
1	1.83	1.56	1.58	–1.24	–6.30	–3.50	2.80	2.76
2	1.46	0.97	1.58	–1.30	–5.71	–3.44	2.27	2.64
3	1.77	1.05	1.94	–1.39	–5.79	–3.35	2.44	2.70
4	1.68	1.59	1.52	–1.36	–6.33	–3.38	2.95	2.70
5	1.57	1.17	1.56	–0.79	–5.91	–3.95	1.96	2.53

[a] Band gaps obtained from electrochemical data. [b] Band gaps obtained from UV/Vis absorption spectrum.

Oxygen-Sensing Properties

The oxygen-sensing properties of this series of complexes were tested by physically incorporating them into MCM-41 and SBA-15 (designated as complex/MCM-41 and complex/SBA-15, respectively) with three loading levels of 40, 60, and 80 mg g⁻¹, respectively. The sensitivity properties of our present samples are discussed on the basis of luminescence intensity quenching.

As can be seen from Figure 4, the powder small-angle X-ray diffraction (SAXRD) measurements reveal that the prepared samples (i.e., 1–4/MCM-41 and 1–4/SBA-15) are structurally mesoporous MCM-41 and SBA-15, respectively.^[13] For the MCM-41 systems, the close d_{100} spacing values of all of these samples indicate that their framework hexagonal ordering was preserved after the introduction of the complexes. Very similar SAXRD results were also obtained in the SBA-15 systems, as shown in Figure 4; all samples exhibit similar patterns typically observed for SBA-15. The UV/Vis absorption spectra of the composite systems show similar profiles to those of pure complexes in dichloromethane (Figure S3, Supporting Information); moreover, the composite samples exhibit characteristic emission of the corresponding complexes. The above-mentioned results prove that the copper(I) complexes were assembled within the mesoporous silica. As depicted in the Stern–Volmer plots of these systems (Figure S4, Supporting Information), the luminescence of the samples can be effectively quenched by oxygen. Owing to weak luminescence properties, attempts to test the oxygen-sensing properties of **5** by using the same method as that used for **1–4** failed.

The Stern–Volmer plots are nonlinear within a wide range of oxygen concentrations. The nonlinearity of these plots in our present work indicates the presence of heterogeneity in the composite system. This phenomenon can be explained by the fact that the luminophore molecules are distributed simultaneously between two or more sites within the silicate support in which one site is more heavily quenched than the others. As a result, the ideal Stern–Volmer equation^[5d,14] is not suitable for the nonlinear Stern–Volmer plots, because the different microheterogeneous sites exhibit different quenching constant (K_{SV}) and unquenched lifetime τ_0 values. In the microheterogeneous solid-based oxygen sensing systems, Demas “two-site” model has been proved to have excellent ability to fit the downward turning of the Stern–Volmer plots.^[5d,15,16] If we change the item “ I_0/I ” in Demas model to “ I/I_0 ”, then the equation takes on the expression given in Equation (1).

$$\frac{I}{I_0} = \frac{f_{01}}{1 + K_{SV1}pO_2} + \frac{f_{02}}{1 + K_{SV2}pO_2} \quad (1)$$

where f_{0i} are the fractional contribution from each oxygen accessible site and K_{SVi} are the associated Stern–Volmer quenching constants for each accessible site. The results of nonlinear fitting are compiled in Table S2 (Supporting Information), from which can be seen that the Demas model is applicable to our data.

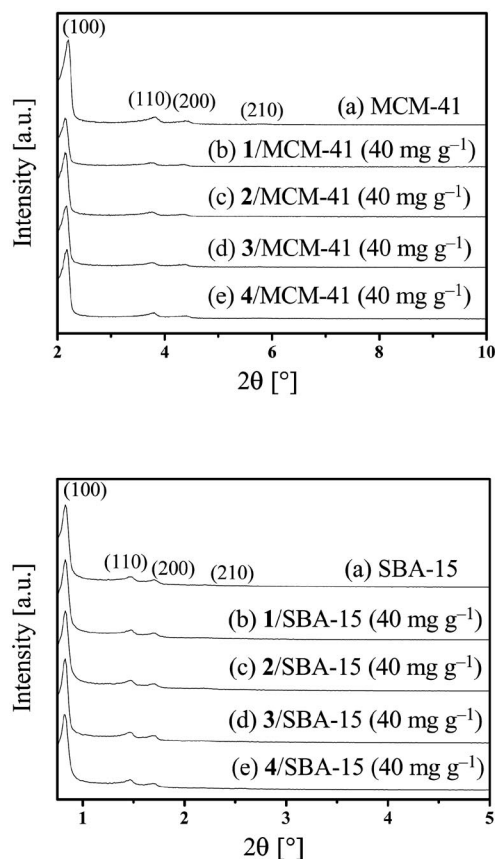


Figure 4. Powder SAXRD spectra of MCM-41 and SBA-15 and the corresponding 40 mg g⁻¹ loading level systems.

The response time (t_{\downarrow}) and recovery time (t_{\uparrow})^[3h] are also very important parameters in evaluating an oxygen sensor. Response property tests were carried out on all of the samples and the values of t_{\downarrow} and t_{\uparrow} are displayed in Table 4. It can be observed that t_{\downarrow} of the MCM-41 system is slightly longer than that of the SBA-15 system, whereas t_{\uparrow} of the former is significantly shorter than that of the latter. We think the difference lies in the nature of the support. The size of the pores in SBA-15 is larger than that in MCM-41; thus, the adsorption and transportation of oxygen in SBA-

Table 4. Values of t_{\downarrow} , t_{\uparrow} , and sensitivity (I_0/I_{100}).

	Loading level [mg g ⁻¹]	t_{\downarrow} [s]		t_{\uparrow} [s]		I_0/I_{100}	
		MCM-41	SBA-15	MCM-41	SBA-15	MCM-41	SBA-15
1	40	5	3	84	181	5.56	6.56
	60	5	3	80	178	7.27	7.44
	80	13	4	60	185	6.53	6.73
2	40	6	3	34	135	2.86	2.47
	60	5	3	36	148	4.40	2.50
	80	8	4	50	158	3.71	5.68
3	40	3	2	60	132	3.72	4.82
	60	3	3	66	113	3.68	4.95
	80	7	3	68	119	4.01	5.51
4	40	6	3	36	139	3.78	4.95
	60	6	3	20	125	3.83	4.63
	80	8	3	39	126	5.95	5.18

15 should be faster than that in MCM-41, so the quenching time of the former is shorter than the latter. When the atmosphere changed from oxygen to nitrogen, it should take more time for the SBA-15 system to desorb the larger amount of oxygen that was adsorbed in the channels tightly (oxygen molecule is notorious for its strong adsorption on silica surface). Consequently, the recovery time of the SBA-15 systems is longer than that of the MCM-41 systems. For both the MCM-41 and SBA-15 systems, the recovery times are longer than the response times. This phenomenon has been rationalized by the above-mentioned fact: the oxygen molecule is well known to be adsorbed strongly on silica surfaces, and thus, the longer recovery time may be attributed to slow desorption of oxygen from the silica surface in the support.

The sensitivity (I_0/I_{100} , where I_0 and I_{100} represent the luminescent intensities in 100% nitrogen and 100% oxygen, respectively) values of all of the samples are also displayed in Table 4. Composite systems containing **1** showed the highest sensitivity whether utilizing MCM-41 or SBA-15 as matrix as a result of its intense emission. Complex **2** encapsulated in MCM-41 with a loading level of 60 mg g⁻¹ exhibits the highest sensitivity, and as for the SBA-15 systems, a loading level of 80 mg g⁻¹ displays the best sensitivity. Complex **3** incorporated into MCM-41 and SBA-15 with a loading of 80 mg g⁻¹ showed higher sensitivity than loadings at the 40 and 60 mg g⁻¹ levels. The same variation trend in sensitivity was also found for systems containing **4**.

We speculate that this complex variation trend in sensitivity can be explained as follows: There are at least two opposite factors affecting the sensitivity of the samples: emission intensity from the probe molecules and adverse interaction between probe molecules (e.g., aggregation). When the loading level is low, the emission from the probe is comparatively weak, which will result in low sensitivity, and when it is high, aggregation between the probe molecules in the pores of the support may become serious. The two opposite factors mentioned above probably affect the sensing properties of the composite systems with different contributions. For samples containing **1**, the influence from the two opposite factors may be equivalent, so sensing properties at a loading level of 60 mg g⁻¹ is the highest among the three. As for **3** and **4**, which exhibit much weaker emission than **1**, composite systems containing them with the highest loading level shows the highest sensitivity, which indicates that the emission intensity factor plays the primary role. In case of complex **2**, it exhibits different variation trends in different supports. When encapsulated in MCM-41, it displays behavior similar to that of **1** (influence from the two opposite factors is almost equivalent): 60 mg g⁻¹ is its optimal loading level, and when incorporated into SBA-15, it takes on the sensitivity variation trend of **3** and **4** (emission intensity is the leading factor).

Conclusions

A series of luminescent copper(I) complexes {[Cu(dpephos)(NN)]BF₄} were synthesized and characterized,

and their photophysical properties are strongly affected by the molecular structure of the NN ligands. Particularly, in view of solid-state emissions at room temperature, the variation trend can be concluded as follows: the more coplanar the NN ligand, the stronger the emission and the higher the emission energy of the corresponding complex. Complexes **1–4** show oxygen-sensing properties upon incorporation into mesoporous silica (MCM-41 and SBA-15). It is environmentally and economically attractive to employ comparatively inexpensive and nontoxic metal complexes in oxygen sensing.

Experimental Section

Starting Materials: Bis[2-(diphenylphosphanyl)phenyl] ether (dpephos), 1,10-phenanthroline monohydrate (phen·H₂O), benzaldehyde, 1-naphthaldehyde, 1-anthraldehyde, and bromoethane were purchased from Aldrich Chemical Co. [Cu(NCCH₃)₄]BF₄ was prepared according to a literature procedure.^[6b]

Synthesis of the NN Ligands

2-Phenyl-1*H*-imidazo[4,5-*f*][1,10]phenanthroline (pip): The pip ligand was synthesized according to reported procedures.^[6c,6d]

1-Ethyl-2-phenyl-1*H*-imidazo[4,5-*f*][1,10]phenanthroline (epip): This compound was synthesized according to a literature procedure with some minor modifications.^[6e] NaH (0.74 g, 20 mmol) was added to anhydrous *N,N*-dimethylformamide (30 mL) in a 100 mL flask; the mixture was stirred violently for 1 h. Then, pip (2.96 g, 10 mmol) was added to the flask, and the mixture was stirred for 1 h. Bromoethane (1.09 g, 10 mmol) was added to the resulting mixture, which was heated at reflux for 24 h, cooled to room temperature, poured into cold water and stirred for 30 min. A pale-purple precipitate was obtained. The crude product was collected by filtration and purified by recrystallization from methanol to give the product (2.14 g, 72%) as a milk-white powder. ¹H NMR (300 MHz, CDCl₃, 25 °C): δ = 9.168 (m, 2 H, 2-H, 9-H), 9.070 (m, 1 H, 7-H), 8.610 (m, 1 H, 4-H), 7.729 (m, 4 H, 10-H, 14-H, 3-H, 8-H), 7.576 (m, 3 H, 11-H, 12-H, 13-H), 4.636 (q, 2 H, CH₂), 1.594 (t, 3 H, CH₃) ppm. C₂₁H₁₆N₄ (324.39): calcd. C 77.76, H 4.97, N 17.27; found C 77.74, H 4.99, N 17.25. IR (KBr pellet): ν̄ = 3055, 2987, 2937, 2879, 1595, 1562, 781, 739, 706, 548 cm⁻¹.

2-(Naphthalen-1-yl)-1*H*-imidazo(4,5-*f*)(1,10)phenanthroline (nip): This compound was synthesized following methods reported in the literature.^[6c,6d,6f] 1-Naphthaldehyde (1.56 g, 10 mmol), 1,10-phenanthroline-5,6-dione (2.10 g, 10 mmol), ammonium acetate (0.15 g, 20 mmol), and acetic acid (30 mL) were added to a 100 mL flask. The mixture was heated at reflux for 12 h. The product (3.25 g, 85%) was obtained as a pale-yellow powder. ¹H NMR (300 MHz, CDCl₃, 25 °C): δ = 11.609 (s, 1 H, N-H), 9.124 (m, 2 H, 2-H, 9-H), 8.786 (m, 1 H, 16-H), 8.535 (m, 1 H, 7-H), 7.942 (m, 3 H, 4-H, 12-H, 13-H), 7.717 (m, 1 H, 10-H), 7.633 (m, 1 H, 11-H), 7.560 (m, 4 H, 3-H, 8-H, 14-H, 15-H) ppm. C₂₃H₁₄N₄ (346.39): calcd. C 79.75, H 4.07, N 16.17; found C 79.73, H 4.06, N 16.19. IR (KBr pellet): ν̄ = 3049, 1608, 1562, 885, 798, 775, 738 cm⁻¹.

1-Ethyl-2-(naphthalen-1-yl)-1*H*-imidazo(4,5-*f*)(1,10)phenanthroline (enip): The synthesis procedure for enip was similar to that of epip, except nip (3.18 g, 10 mmol) was used in place of pip. The product (3.14 g, 74%) was obtained as a milk-white powder. ¹H NMR (300 MHz, CDCl₃, 25 °C): δ = 9.176 (m, 2 H, 2-H, 9-H), 9.090 (d, *J* = 4.5 Hz, 1 H, 16-H), 8.654 (m, 1 H, 7-H), 8.089 (m, 1 H, 4-H), 7.987 (m, 1 H, 13-H), 7.721 (m, 3 H, 10-H, 11-H, 12-H), 7.669 (m,

1 H, 8-H), 7.543 (m, 2 H, 3-H, 15-H), 7.489 (m, 1 H, 14-H), 4.421 (q, 2 H, CH₂), 1.435 (t, 3 H, CH₃) ppm. C₂₅H₁₈N₄ (374.45): calcd. C 80.19, H 4.85, N 14.96; found C 80.17, H 4.86, N 14.98. IR (KBr pellet): $\tilde{\nu}$ = 3050, 2987, 1616, 1562, 875, 793, 739 cm⁻¹.

2-(Anthracen-9-yl)-1-ethyl-1H-imidazo(4,5-f)(1,10)phenanthroline (aeip): The synthesis procedure for aeip was similar to that of enip, except 1-anthrathaldehyde (2.36 g, 10 mmol) was used in place of 1-naphthaldehyde. ¹H NMR (300 MHz, CDCl₃, 25 °C): δ = 9.256 (m, 2 H, 2-H, 9-H), 9.148 (m, 1 H, 10-H), 8.718 (m, 2 H, 4-H, 7-H), 8.151 (m, 2 H, 14-H, 15-H), 7.777 (m, 2 H, 11-H, 18-H), 7.571 (m, 4 H, 3-H, 8-H, 16-H, 13-H), 7.468 (m, 2 H, 12-H, 17-H), 4.329 (q, 2 H, CH₂), 1.320 (t, 3 H, CH₃) ppm. C₂₉H₂₀N₄ (424.51): calcd. C 82.05, H 4.75, N 13.20; found C 82.03, H 4.77, N 13.19. IR (KBr pellet): $\tilde{\nu}$ = 3052, 2985, 2931, 1627, 1598, 1562, 736, 688, 661, 688 cm⁻¹.

Synthesis of Complexes 1–5: The five complexes were synthesized following a procedure similar to that reported in the literature.^[6a] A typical procedure is outlined for **1**. The synthesis procedures for **2–5** were essentially identical to that described for **1**, only the quantities of the NN ligands differed.

Complex 1: A 100 mL flask was charged with [Cu(CH₃CN)₄]BF₄ (31 mg, 0.1 mmol), dpephos (54 mg, 0.1 mmol) and dichloromethane (10 mL), and the mixture was stirred for 1 h. Then, pip (30 mg, 0.1 mmol) was added, and the mixture was stirred for 1 h. After evaporation of the solvent, the product (80 mg, 70%) was obtained as a yellow powder. ¹H NMR (300 MHz, CDCl₃, 25 °C): δ = 9.253 (d, *J* = 5.4 Hz, 2 H, 2-H, 9-H), 8.547 (d, *J* = 5.5 Hz, 2 H, 4-H, 7-H), 8.436 (d, *J* = 5.7 Hz, 2 H, 10-H, 14-H), 7.629 (m, 2 H, 3-H, 8-H), 7.580 (m, 2 H, 11-H, 13-H), 7.472 (t, 1 H, 12-H), 7.296 (m, 2 H, 31-H, 34-H), 7.240 (m, 4 H, 29-H, 32-H, 33-H, 36-H), 7.097 (t, 12 H, 20-H, 21-H, 22-H, 25-H, 26-H, 27-H, 38-H, 39-H, 40-H, 43-H, 44-H, 45-H), 6.980 (m, 8 H, 19-H, 23-H, 24-H, 28-H, 37-H, 41-H, 42-H, 46-H), 6.811 (m, 2 H, 30-H, 35-H) ppm. C₅₅H₄₀BCuF₄N₄OP₂ (985.25): calcd. C 67.05, H 4.09, N 5.69; found C 67.03, H 4.11, N 5.66. IR (KBr pellet): $\tilde{\nu}$ = 3483, 3055, 1612, 1433, 1265, 1074, 804, 737, 694, 515 cm⁻¹.

Complex 2: The epip ligand (32 mg, 0.1 mmol) was used. Yield: 85 mg (73%). ¹H NMR (300 MHz, CDCl₃, 25 °C): δ = 9.112 (m, 2 H, 2-H, 9-H), 8.696 (d, *J* = 6.0 Hz, 1 H, 7-H), 8.656 (d, *J* = 5.5 Hz, 1 H, 4-H), 7.985 (m, 1 H, 12-H), 7.775 (m, 2 H, 10-H, 14-H), 7.618 (m, 4 H, 3-H, 8-H, 11-H, 13-H), 7.312 (t, 2 H, 31-H, 34-H), 7.238 (m, 4 H, 21-H, 26-H, 39-H, 44-H), 7.113 (m, 10 H, 20-H, 22-H, 25-H, 27-H, 38-H, 40-H, 43-H, 45-H, 30-H, 35-H), 6.989 (t, 10 H, 19-H, 23-H, 24-H, 28-H, 29-H, 36-H, 37-H, 41-H, 42-H, 46-H), 6.781 (m, 2 H, 29-H, 36-H), 4.832 (q, 2 H, CH₂), 1.619 (t, 3 H, CH₃) ppm. C₅₇H₄₄BCuF₄N₄OP₂ (1013.30): calcd. C 67.56, H 4.38, N 5.53; found C 67.54, H 4.40, N 5.55. IR (KBr pellet): $\tilde{\nu}$ = 3469, 3057, 2943, 2875, 1626, 1566, 1435, 1263, 1055, 804, 740, 696, 513 cm⁻¹.

Complex 3: The nip ligand (35 mg, 0.1 mmol) was used. Yield: 100 mg (83%). ¹H NMR (300 MHz, CDCl₃, 25 °C): δ = 12.673 (s, 1 H, N-H), 9.281 (m, 3 H, 2-H, 9-H, 16-H), 8.566 (m, 2 H, 4-H, 7-H), 8.338 (m, 1 H, 13-H), 7.903 (m, 2 H, 10-H, 12-H), 7.654 (m, 4 H, 3-H, 8-H, 14-H, 15-H), 7.524 (m, 1 H, 11-H), 7.304 (m, 2 H, 31-H, 34-H), 7.231 (m, 4 H, 21-H, 26-H, 39-H, 44-H), 7.114 (m, 8 H, 20-H, 22-H, 25-H, 27-H, 38-H, 40-H, 43-H, 45-H), 7.074 (m, 4 H, 30-H, 32-H, 33-H, 35-H), 7.000 (t, 8 H, 19-H, 23-H, 24-H, 28-H, 37-H, 41-H, 42-H, 46-H), 6.805 (m, 2 H, 29-H, 36-H) ppm. C₅₉H₄₂BCuF₄N₄OP₂ (1035.31): calcd. C 68.45, H 4.09, N 5.41; found C 68.43, H 4.07, N 5.43. IR (KBr pellet): $\tilde{\nu}$ = 3504, 3055, 1564, 1433, 1263, 1070, 771, 741, 696, 509 cm⁻¹.

Complex 4: The enip ligand (37 mg, 0.1 mmol) was used. Yield: 103 mg (84%). ¹H NMR (300 MHz, CDCl₃, 25 °C): δ = 9.128 (m, 2 H, 2-H, 9-H), 8.742 (d, *J* = 5.4 Hz, 2 H, 4-H, 7-H), 8.109 (d, *J* = 6.0 Hz, 1 H, 16-H), 7.999 (d, *J* = 6.0 Hz, 1 H, 13-H), 7.617 (m, 7 H, 3-H, 8-H, 10-H, 11-H, 12-H, 14-H, 15-H), 7.318 (m, 6 H, 21-H, 26-H, 31-H, 34-H, 39-H, 44-H), 7.145 (m, 8 H, 20-H, 22-H, 25-H, 27-H, 38-H, 40-H, 43-H, 45-H), 6.998 (m, 12 H, 19-H, 23-H, 24-H, 28-H, 29-H, 32-H, 33-H, 36-H, 37-H, 41-H, 42-H, 46-H), 6.285 (m, 2 H, 29-H, 36-H), 4.593 (q, 2 H, CH₂), 1.445 (t, 3 H, CH₃) ppm. C₆₁H₄₆BCuF₄N₄OP₂ (1063.36): calcd. C 68.90, H 4.36, N 5.27; found C 68.92, H 4.34, N 5.25. IR (KBr pellet): $\tilde{\nu}$ = 3055, 2995, 1597, 1566, 1435, 1261, 1058, 874, 804, 777, 741 cm⁻¹.

Complex 5: The aeip ligand (42 mg, 0.1 mmol) was used. Yield: 109 mg (86%). ¹H NMR (300 MHz, CDCl₃, 25 °C): δ = 9.266 (m, 1 H, 9-H), 9.186 (d, *J* = 6.3 Hz, 1 H, 2-H), 8.811 (d, *J* = 5.5 Hz, 1 H, 7-H), 8.762 (s, 1 H, 4-H), 8.683 (d, *J* = 5.5 Hz, 1 H, 10-H), 8.167 (d, *J* = 6.3 Hz, 2 H, 14-H, 15-H), 8.105 (m, 1 H, 11-H), 7.648 (m, 1 H, 18-H), 7.548 (m, 2 H, 3-H, 8-H), 7.481 (m, 4 H, 12-H, 13-H, 16-H, 17-H), 7.324 (m, 6 H, 21-H, 26-H, 31-H, 34-H, 39-H, 44-H), 7.167 (m, 8 H, 20-H, 22-H, 25-H, 27-H, 38-H, 40-H, 43-H, 45-H), 7.095 (d, *J* = 6.3 Hz, 2 H, 32-H, 33-H), 7.017 (t, 10 H, 19-H, 23-H, 24-H, 28-H, 37-H, 41-H, 42-H, 46-H, 30-H, 35-H), 6.817 (m, 2 H, 29-H, 36-H), 4.472 (q, 2 H, CH₂), 1.347 (t, 3 H, CH₃) ppm. C₆₅H₄₈BCuF₄N₄OP₂ (1113.42): calcd. C 70.12, H 4.35, N 5.03; found C 70.14, H 4.33, N 5.05. IR (KBr pellet): $\tilde{\nu}$ = 3054, 2931, 2859, 1627, 1564, 1429, 1261, 1054, 802, 738, 688, 509 cm⁻¹.

Preparation of Mesoporous Silica MCM-41, SBA-15, and the Composite Systems: Mesoporous silica MCM-41 and SBA-15 were prepared following the reported procedure with some minor modifications.^[17] As can be seen from Figure 4, the SAXRD measurements reveal that blank MCM-41 show three well-resolved broad Bragg reflections that can be indexed as *d*₁₀₀, *d*₁₁₀, and *d*₂₀₀, which are the characteristics of a well-ordered hexagonal mesostructure.^[13a] SAXRD results of the undoped SBA-15 consists of a strong (100) reflection at a low-angle region ranging from 0.7 to 1° (2θ) and three small peaks (110, 200, 210) located at the higher angle range.^[13b] The pore size of SBA-15 is larger than that of MCM-41. Complex/MCM-41 and complex/SBA-15 composite materials were prepared respectively by the following procedure. In a typical preparation, **1** (4 mg) was added into dichloromethane (10 mL), and the mixture was stirred for 1 h. Then MCM-41 or SBA-15(0.10 g) was added into the dichloromethane solution of **1**. The mixture was stirred for 24 h at room temperature and filtered. The obtained powder was washed several times with the solvent until no **1** existed in the filtrate. The powder was dried in air, and target sample **1**/MCM-41 or **1**/SBA-15 was obtained. The samples with different loading levels (40, 60, and 80 mg g⁻¹ MCM-41 or SBA-15) were prepared by altering the concentration of initial solution of **1**, **2**, **3**, and **4**, respectively.

Physical Measurements: The IR spectra were acquired with a Magna560 FTIR spectrophotometer. Element analyses were performed with a Vario Element Analyzer. ¹H NMR spectra were obtained with a Bruker Avance 300 MHz spectrometer with tetramethylsilane as the internal standard. The absorption spectra were recorded with a Shimadzu Model 3100 spectrometer and the photoluminescence spectra were obtained by a Hitachi F-4500 fluorescence spectrophotometer equipped with a monochromator (resolution: 0.2 nm) and a 150W Xe lamp as the excitation source. The excited-state lifetimes were determined by using a conventional Nd:YAG (neodymium yttrium aluminum garnet) laser system. The photoluminescence quantum yield is defined as the number of photons emitted per photon absorbed by the system and was measured

with an integrating sphere by a literature method.^[10] The SAXRD data were collected with a Bruker D8 Discover diffractometer equipped with Cu target ($\lambda = 1.5406 \text{ \AA}$). The scanning range was $1\text{--}10^\circ$ with 0.01° step and scanning speed was 1 s step^{-1} .

Crystallography: Yellow single crystals of **3**· $6\text{C}_2\text{H}_5\text{OH}$ and **4**· $2\text{C}_2\text{H}_5\text{OH}$ suitable for X-ray diffraction studies were obtained by slow evaporation from dichloromethane/ethanol solution and measured with a Bruker Smart Apex CCD single-crystal diffractometer by using $\lambda(\text{Mo-K}\alpha)$ radiation (0.7107 \AA at 273 K). An empirical absorption was based on the symmetry-equivalent reflections and applied to the data by using the SADABS program. The structure was solved by using the SHELXL-97 program.^[18] The crystallographic refinement parameters of the crystals are summarized in Table S1 (Supporting Information), whereas selected bond lengths and angles were given in Table 1. CCDC-717860 (for **3**· $6\text{C}_2\text{H}_5\text{OH}$), and -717861 (for **4**· $2\text{C}_2\text{H}_5\text{OH}$) contain the supplementary crystallographic data for this paper. These data can be obtained free of charge from The Cambridge Crystallographic Data Centre via www.ccdc.cam.ac.uk/data_request/cif.

Thermal Analysis: TGA was performed on a ca. 2 mg sample of **1**–**5** by using a Perkin–Elmer thermal analyzer. The samples were dried under vacuum at 56.5°C before being heated from 40 to 600°C at a heating rate of $10.0^\circ\text{C min}^{-1}$. A flowrate of 10 mL min^{-1} of dry nitrogen was used to purge the sample at all times.

Oxygen-Sensing Properties Test: Oxygen-sensing properties of our samples were discussed on the basis of luminescence intensity quenching instead of the excited-state lifetime, because it is hard to obtain precise excited-state lifetime values with a conventional flashlamp-based time-correlated photon counting system.^[5d] The excitation wavelength of all samples was 400 nm . In the measurement of Stern–Volmer plots, oxygen and nitrogen were mixed at different concentrations via gas flow controllers and passed directly to the sealed gas chamber. We typically allowed 1 min between changes in the N_2/O_2 concentration to ensure that a new equilibrium point had been established. Equilibrium was evident when the luminescence intensity remained constant. The sensor response curves were obtained by using a similar method. The experiments were carried out in the dark at room temperature.

Supporting Information (see footnote on the first page of this article): Crystal data and refinement details for **3**· $6\text{C}_2\text{H}_5\text{OH}$ and **4**· $2\text{C}_2\text{H}_5\text{OH}$; Demas model oxygen-quenching fitting parameters for the composite systems; absorption spectra of **1**–**5** the ligands; solid-state photoluminescence lifetime decay curve of **1**–**4**; UV/Vis absorption spectra comparison between **1**–**4** and the corresponding composite systems; Stern–Volmer plots for the composite systems at different oxygen concentrations.

Acknowledgments

The authors are grateful for the financial support of the Chinese Academy of Sciences (One Hundred Talents Project) and the NSFC (Grant no. 50872130).

[1] a) A. Lavie-Cambot, M. Cantuel, Y. Leydet, G. Jonusauskas, D. M. Bassani, N. D. McClenaghan, *Coord. Chem. Rev.* **2008**, *252*, 2572–2584; b) N. Armaroli, G. Accorsi, F. Cardinali, A. Listorti, *Top. Curr. Chem.* **2007**, *280*, 69–115; c) D. R. McMillin, K. M. McNett, *Chem. Rev.* **1998**, *98*, 1201–1219; d) N. Armaroli, *Chem. Soc. Rev.* **2001**, *30*, 113–124; e) D. V. Scaltrito, D. W. Thompson, J. A. O’Callaghan, G. J. Meyer, *Coord. Chem. Rev.* **2000**, *208*, 243–266; f) L. Yang, J. Feng, A. Ren, M. Zhang, Y. Ma, X. Liu, *Eur. J. Inorg. Chem.* **2005**, *10*, 1867–

- 1869; g) N. Armaroli, G. Accorsi, G. Bergamini, P. Ceroni, M. Holler, O. Moudam, C. Duhayon, B. Delavaux-Nicot, J. F. Nierengarten, *Inorg. Chim. Acta* **2007**, *360*, 1032–1042.
- [2] a) W. Jia, T. McCormick, Y. Tao, J. Lu, S. Wang, *Inorg. Chem.* **2005**, *44*, 5706–5712; b) A. Tsuboyama, K. Kuge, M. Furugori, S. Okada, M. Hoshino, K. Ueno, *Inorg. Chem.* **2007**, *46*, 1992–2001; c) Q. Zhang, Q. Zhou, Y. Cheng, L. Wang, D. Ma, X. Jing, F. Wang, *Adv. Mater.* **2004**, *16*, 432–436; d) S. Zhao, R. Wang, S. Wang, *Inorg. Chem.* **2006**, *45*, 5830–5840.
- [3] a) J. N. Demas, B. A. Degraff, *Coord. Chem. Rev.* **2001**, *211*, 317–351; b) S. M. Borisov, A. S. Vasylevska, C. Krause, O. S. Wolfbeis, *Adv. Funct. Mater.* **2006**, *16*, 1536–1542; c) S. M. Borisov, O. S. Wolfbeis, *Anal. Chem.* **2006**, *78*, 5094–5101; d) S. M. Borisov, V. V. Vasil’ev, *Russ. J. Anal. Chem.* **2004**, *59*, 155–159; e) S. H. Cheng, C. H. Lee, C. S. Yang, F. G. Tseng, C. Y. Mou, L. W. Lo, *J. Mater. Chem.* **2009**, *19*, 1252–1257; f) B. Meier, T. Werner, I. Klimant, O. S. Wolfbeis, *Sens. Actuators B* **1995**, *29*, 240–245; g) S. M. Borisov, G. Nuss, I. Klimant, *Anal. Chem.* **2008**, *80*, 9435–9442; h) C. Huo, H. Zhang, H. Zhang, H. Zhang, B. Yang, P. Zhang, Y. Wang, *Inorg. Chem.* **2006**, *45*, 4735–4742.
- [4] M. T. Miller, T. B. Karpishin, *Sens. Actuators B* **1999**, *61*, 222–224.
- [5] a) A. S. Kocincova, S. Nagl, S. Arain, C. Krause, S. M. Borisov, M. Arnold, O. S. Wolfbeis, *Biotechnol. Bioeng.* **2008**, *100*, 430–438; b) M. C. Moreno-Bondi, O. S. Wolfbeis, M. J. P. Leiner, B. P. H. Schaffar, *Anal. Chem.* **1990**, *62*, 2377–2380; c) O. S. Wolfbeis, L. J. Weis, M. J. P. Leiner, W. E. Ziegler, *Anal. Chem.* **1988**, *60*, 2028–2030; d) B. Lei, B. Li, H. Zhang, Sh. Lu, Z. Zheng, W. Li, Y. Wang, *Adv. Funct. Mater.* **2006**, *16*, 1883–1891.
- [6] a) S. M. Kuang, D. G. Cuttall, D. R. McMillin, P. E. Fanwick, R. A. Walton, *Inorg. Chem.* **2002**, *41*, 3313–3322; b) G. J. Kubas, *Inorg. Synth.* **1979**, *19*, 90–92; c) E. A. Steck, A. R. Day, *J. Am. Chem. Soc.* **1943**, *65*, 452–456; d) C. W. Jiang, H. Chao, R. H. Li, H. Li, L. N. Ji, *Polyhedron* **2001**, *20*, 2187–2193; e) H. Xin, F. Y. Li, M. Guan, C. H. Huang, M. Sun, K. Z. Wang, Y. A. Zhang, L. P. Jin, *J. Appl. Phys.* **2003**, *94*, 4729–4731; f) M. J. Han, L. H. Gao, K. Z. Wang, *New J. Chem.* **2006**, *30*, 208–214.
- [7] a) N. M. Shavaleev, H. Adams, J. A. Weinstein, *Inorg. Chim. Acta* **2007**, *360*, 700–704; b) Z. Q. Bian, K. Z. Wang, L. P. Jin, *Polyhedron* **2002**, *21*, 313–319.
- [8] N. H. Damrauer, T. R. Bousie, M. Devenney, J. K. McCusker, *J. Am. Chem. Soc.* **1997**, *119*, 8253–8268.
- [9] L. Huang, K. Z. Wang, C. H. Huang, F. Y. Li, Y. Y. Huang, *J. Mater. Chem.* **2001**, *11*, 790–793.
- [10] M. S. Wrighton, D. S. Ginley, D. L. Morse, *J. Phys. Chem.* **1974**, *78*, 2229–2233.
- [11] a) P. Federlin, J. M. Kern, A. Rastegar, C. Dieterich-Buchecker, P. A. Marnot, J. P. Sauvage, *New J. Chem.* **1990**, *14*, 9–12; b) M. Ruthkosky, F. N. Castellano, G. J. Meyer, *Inorg. Chem.* **1996**, *35*, 6406–6412; c) Y. Rio, G. Accorsi, N. Armaroli, D. Felder, E. Levillain, J. F. Nierengarten, *Chem. Commun.* **2002**, 2830–2831.
- [12] a) A. J. Nozik, R. Meming, *J. Phys. Chem.* **1996**, *100*, 13061–13078; b) C. Q. Ma, L. Q. Zhang, J. H. Zhou, X. S. Wang, B. W. Zhang, Y. Cao, P. Bugnon, M. Schaer, F. Nuesch, D. Q. Zhang, Y. Qiu, *J. Mater. Chem.* **2002**, *12*, 3481–3486.
- [13] a) J. S. Beck, J. C. Vartuli, W. J. Roth, M. E. Leonowicz, C. T. Kresge, K. D. Schmitt, C. T.-W. Chu, D. H. Olson, E. W. Sheppard, S. B. McCullen, J. B. Higgins, J. L. Schlenker, *J. Am. Chem. Soc.* **1992**, *114*, 10834–10843; b) D. Y. Zhao, J. L. Feng, Q. S. Huo, N. Melosh, G. H. Fredrickson, B. F. Chmelka, G. D. Stucky, *Science* **1998**, *279*, 548–552.
- [14] V. O. Stern, M. Volmer, *Phys. Z.* **1919**, *20*, 183–188.
- [15] a) Y. Tang, E. C. Tehan, Z. Y. Tao, F. V. Bright, *Anal. Chem.* **2003**, *75*, 2407–2413; b) W. Y. Xu, R. C. McDonough, B. Langsdorf, J. N. Demas, B. A. DeGraff, *Anal. Chem.* **1994**, *66*,

- 4133–4141; c) J. N. Demas, B. A. Deora, W. Y. Xu, *Anal. Chem.* **1995**, *67*, 1377–1380.
- [16] B. W.-K. Chu, V. W. W. Yam, *Langmuir* **2006**, *22*, 7437–7443.
- [17] B. F. Lei, B. Li, H. R. Zhang, L. M. Zhang, W. L. Li, *J. Phys. Chem. C* **2007**, *111*, 11291–11301.
- [18] a) G. M. Sheldrick, *SHELXTL*, version 5.10, Siemens Analytical X-ray Instruments Inc., Madison, WI, **1998**; b) *SMART* and *SAINT*, Siemens Analytical X-ray Instruments Inc., Madison, WI, **1995**; c) G. M. Sheldrick, *SADABS*, University of Göttingen, Göttingen, Germany, **1996**.

Received: February 4, 2009
Published Online: April 16, 2009